

Spatial-Separated Curve Rendering Network for Efficient and High-Resolution Image Harmonization

Jingtang Liang^{1*}, Xiaodong Cun^{1,2*}, Chi-Man Pun^{1†}

¹ University of Macau, ² Tencent AI Lab
mb95464@umac.mo, shadowcun@tencent.com, cmpun@umac.mo

Abstract

Image harmonization aims to modify the color of the composited region with respect to the specific background. Previous works model this task as a pixel-wise image-to-image translation using UNet family structures. However, the model size and computational cost limit the ability of their models on edge devices and higher-resolution images. To this end, we propose a novel spatial-separated curve rendering network (S²CRNet) for efficient and high-resolution image harmonization for the first time. In S²CRNet, we firstly extract the spatial-separated embeddings from the thumbnails of the masked foreground and background individually. Then, we design a curve rendering module (CRM), which learns and combines the spatial-specific knowledge using linear layers to generate the parameters of the pixel-wise curve mapping in the foreground region. Finally, we directly render the original high-resolution images using the learned color curve. Besides, we also make two extensions of the proposed framework via the Cascaded-CRM and Semantic-CRM for cascaded refinement and semantic guidance, respectively. Experiments show that the proposed method reduces more than 90% parameters compared with previous methods but still achieves the state-of-the-art performance on both synthesized iHarmony4 and real-world DIH test set. Moreover, our method can work smoothly on higher resolution images in real-time which is more than 10× faster than the existing methods. The code and pre-trained models will be made available and released at <https://github.com/stefanLeong/S2CRNet>.

Introduction

Image composition (or image splicing in multimedia security) is a popular and necessary tool for image editing. However, in addition to the serrated edges caused by the irregular borders, the “style” disharmony occurs when we directly copy source regions (foreground) to the host image (background). The disharmony will degrade the quality of the composited images, which also can be distinguished by the human eyes easily. In general, handling this gap requires the professional editing of the well-knowledged experts. Thus, the task of image harmonization aims to squeeze this gap by leveraging some advanced algorithms, which also has a

*These authors contributed equally.

†Corresponding Author

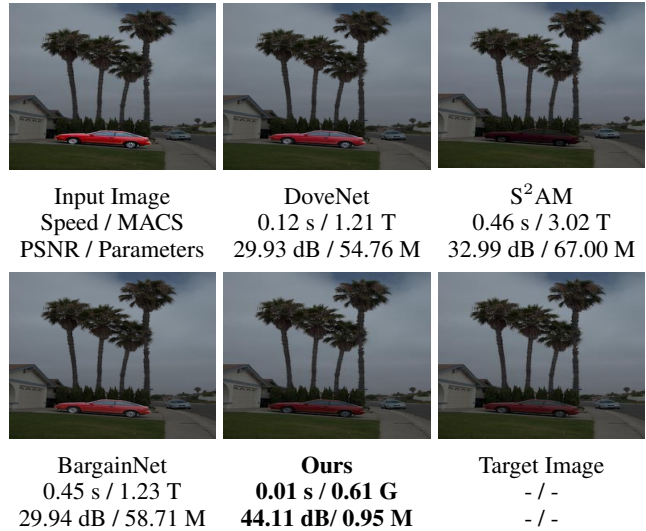


Figure 1: Given a high-resolution image (originally 2048×2048 in this example), our method show many advantages compared with other methods, including the running speed, computational cost (MACS)), performance and model size.

broad impact on image editing, relighting and augmented reality (Zhou et al. 2019; Lee, Pfister, and Yang 2019).

Traditional image harmonization methods intend to manually adjust and modify the specific features in the composite images, such as color (Lalonde and Efros 2007; Reinhard et al. 2001), illumination (Xue et al. 2012) and texture (Sunkavalli et al. 2010), *etc.*. However, the hand-crafted and statistic low-level features cannot work well for the diverse composite images in complicated real world. Since the deep convolutional neural network (CNN) has reached impressive performance in many computer vision tasks, several attempts have also been made to address image harmonization tasks. For example, by considering the semantic clues, (Tsai et al. 2017) propose an end-to-end harmonization framework and (Sofiiuk, Popenova, and Konushin 2021) propose a semantic guided network for image harmonization by combining a solid pre-trained semantic segmentation network. Then, to learn the foreground specifically, (Cun and Pun 2020a) propose a spatial-separated attention module (S²AM) inside the UNet structure and (Hao, Iizuka,

and Fukui 2020) extend S²AM as a feature map modulation module. Later, DoveNet (Cong et al. 2020) designs a novel domain verification discriminator to identify the composite and natural foreground regions by generative adversarial network (GAN (Goodfellow et al. 2014)), while BargainNet (Cong et al. 2021) extracts the domain-aware features to guide further harmonization. In summary, all existing CNN methods consider the image harmonization models as encoder-decoder based structures (Ronneberger, Fischer, and Brox 2015; Isola et al. 2017). Thus, as shown in Figure 1, the speed and computational cost are sensitive to image resolution because those structures require to predict the pixel-wise results. Besides, their model sizes are too large for the edge devices, such as mobile phone. The problems mentioned above restrict the applying range of their methods since the real-world images editing are in any resolution.

Differently, in this paper, we rethink the image harmonization in a totally different way: Reviewing the image harmonization process in image editing software (*e.g.* PhotoShop), experts tend to adjust the global properties (color curve, illuminant, *etc.*) over the whole images rather than the pixel-wise color adjustment. Thus, the global editing can be enabled by considering the properties as the mapping function of the pixels intensities. Moreover, this global adjustment is reliably efficient in any resolution images without extra expense of computational cost.

To make the proposed method efficient on images at any resolutions, we model the observations above by learning parameters of the *global editing curves* of the composite foreground. Hence, a novel curve rendering module (CRM) is designed to produce the image-adaptive parameters of the curves that we will use to render the composite image. Specifically, we first separate the composite image into foreground/background regions using the given foreground mask. Then, we extract the global high-level features from both regions by a shared SqueezeNet (Iandola et al. 2016) pre-trained on ImageNet (Deng et al. 2009). Particularly in CRM, the extracted features from foreground/background are learnt by a single layer linear projection for each region separately. Finally, the combination of these two spatial-specific features will be represented as the parameters of color curves, and we render the original foreground for each color channel with the approximate curves we learned.

Furthermore, we also make two extensions to the proposed framework. On one hand, we propose *semantic-CRM*. Since different foregrounds represent different categories, we learn the class-aware feature embeddings for each category individually by the user-guided foreground semantic encoding. On the other hand, we propose the *cascaded-CRM*, which is also inspired by the photo editing software since the image editing process generally contains multiple steps. In our implementation, we predict different domain embedding to achieve this goal via a cascaded prediction. Benefit by the proposed framework, our method shows a significantly better performance than previous state-of-the-art image harmonization networks with only 2% of the parameters. Besides, our method can also run more than 10× faster than previous methods on high-resolution images (2048 × 2048).

Our main contributions are summarized as follows:

- We propose a novel spatial-separated curve rendering network (S²CRNet). The **first** network structure for both efficient and high-resolution image harmonization.
- We show the extension ability of our curve rendering module (CRM) in the proposed S²CRNet via the Cascaded-CRM and Semantic-CRM.
- Experiments show that our method can achieve state-of-the-art performance and run much faster than the previous methods, while using fewer parameters and lower computational costs.

Related Works

Image Harmonization. Traditional image harmonization methods aim at improving composite images via low-level appearance features, such as manually adjusting global color distributions (Cohen-Or et al. 2006; Bychkovsky et al. 2011), applying gradient domain composition (Jia et al. 2006; Pérez, Gangnet, and Blake 2003) or manipulating multi-scale transformation and statistical analysis (Sunkavalli et al. 2010). Although these methods achieve preliminary results in harmonization tasks, the realism of the composite images cannot be visually guaranteed.

As the deep learning approaches has been successfully applied to the computer vision tasks, (Zhu et al. 2015) back-propagate a pre-trained visual discriminator model to change the appearance harmony of the composite images. Later, further researches consider this task as an image to image translation problem. For example, additional semantic decoder (Tsai et al. 2017) and pre-trained semantic feature (Sofiiuk, Popenova, and Konushin 2021) are used to ensure the semantic consistence between the composite inputs and harmonized outputs. Another noticeable idea is to model the differences between the foreground and background with the given mask. For example, novel spatial-separated attention module (Cun and Pun 2020a; Hao, Iizuka, and Fukui 2020) under image-to-image translation framework; Domain-guided features as the discriminator of GAN (Cong et al. 2020) and as additional input (Cong et al. 2021); masked-guided spatial normalizations (Ling et al. 2021; Guo et al. 2021) for the foreground and background respectively. However, all the previous deep networks still model this task as a pixel-wise image to image translation problem using an encoder-decoder structure, which suffers from computational inefficiency and may degrade the performance and visual quality on high-resolution inputs.

Efficient Neural Network. Efficient networks designed for edge devices have also been widely-discussed in computer vision tasks (Howard et al. 2017). For image enhancement, (Gharbi et al. 2017) introduce the deep bilateral learning for high-resolution and real-time image processing on mobile devices. Also, learning the image-adaptive global style features shows promising results in Exposure (Hu et al. 2018) and 3DLUT (Zeng et al. 2020). Since our task can be considered as a regional image enhancement problem, it is natural to leverage the global style features to image harmonization tasks. However, image harmonization methods rely

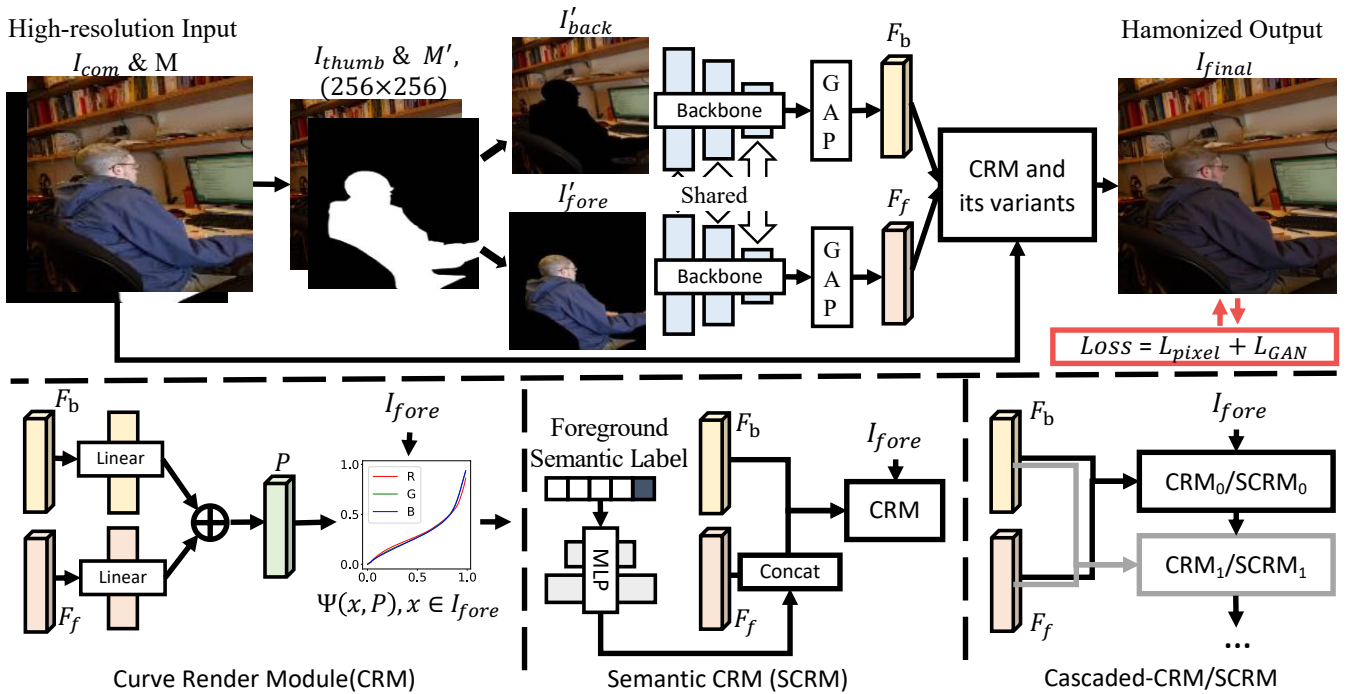


Figure 2: The overview of the S²CRNet, including CRM and its two variants: SCRM and Cascaded-CRM/SCRM.

on regional modification under the guidance of the background. Thus, we design a novel network structure and learn global mapping functions for efficient and high-resolution image harmonization.

Method

In this section, we introduce Spatial-Separated Curve Rendering Network (S²CRNet) for efficient and high-resolution image harmonization. First, we show the overall network structure. Then, we give the details of Curve Rendering Module (CRM) and its variants, which are the key components in S²CRNet, including CRM, *Semantic-CRM* (SCRM) and their cascaded extensions. Finally, we discuss the loss functions.

Overall Network Structure

As shown in Figure 2, given a high-resolution composite image $I_{com} \in \mathbb{R}^{3 \times H \times W}$ and its binary mask $M \in \mathbb{R}^{1 \times H \times W}$ of the corresponding foreground, for fast inference, we first get the thumbnail of the image $I_{thumb} \in \mathbb{R}^{3 \times h \times w}$ and the mask $M' \in \mathbb{R}^{1 \times h \times w}$ by down-sampling I_{com} and M with a factor of H/h . Then, for the spatial-separated feature encoding, we segment the thumbnail image I_{thumb} into foreground and background via the mask M' and inverse mask $M'_{inv} = 1 - M'$, respectively. Next, given the foreground $I_{fore} = I_{thumb} \times M'$ and background $I_{back} = I_{thumb} \times M'_{inv}$ images, we use a shared domain encoder Φ to extract the spatial-separated features for foreground and background respectively. Here, we choose the SqueezeNet (Iandola et al. 2016) feature extractor that is pre-trained on ImageNet (Deng et al. 2009) as the domain encoder (backbone).

SqueezeNet is built up by the stack of *Fire* blocks to maintain good balance between the efficiency and effectiveness, which is also good at capturing the color representations (Yu et al. 2020; Hu, Wang, and Lin 2017). As for feature extractor, we only use the first 12 layers to get deeper color feature embeddings.

After obtaining the embedding foreground $F_{fore} \in \mathbb{R}^{D \times h' \times w'}$ and background $F_{back} \in \mathbb{R}^{D \times h' \times w'}$ features from the domain encoder, we squeeze the foreground/background feature dimensionally via the global average pooling to avoid the influence of spatial information. Then, foreground $F_f \in \mathbb{R}^D$ and background $F_b \in \mathbb{R}^D$ are learnt to generate the parameters of the color curve and render the channel-wise color curve via the proposed *Curve Rendering Module* automatically. We will discuss the details and its variants in the later sections.

Curve Rendering Modules (CRM) and its Variants

In this section, we first introduce the basic idea behind the proposed network via the *Curve Rendering Module* (CRM), which is the key components of our proposed methods. Then, we discuss two different extensions using the semantic label and recurrent refinement.

Curve Rendering Module As shown in Figure 2, given the global features $F_f \in \mathbb{R}^D$ and $F_b \in \mathbb{R}^D$ from the foreground and background, we first embed these features using single linear layer $\phi_f(\cdot)/\phi_b(\cdot)$ for foreground/background correspondingly. Next, we combine $\phi_f(F_f)$ and $\phi_b(F_b)$ together as P because the foreground should be harmonized according to the related background. Then, as shown in the Figure 3, we denote P as the channel-wise parameters

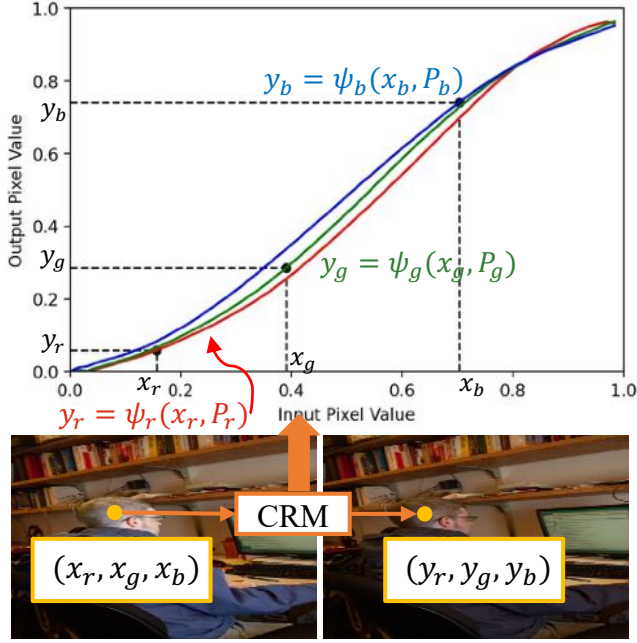


Figure 3: CRM maps the input pixels to the target using curve rendering function $\psi(\cdot)$, where the parameters P of $\psi(\cdot)$ are learnt from the deep domain encoders.

of the curve function for composite foreground. Since the curve is a continuous function respect to the intensity levels, similar to (Hu et al. 2018), we make it differentiable by quantizing the intensity of the images to L levels and denoting P as the parameters of each channel. Mathematically, to learn the curve rendering module for the foreground of RGB image channel I_{fore}^c , $c \in \{R, G, B\}$, the color curve of each channel can be represented as a L level piece-wise function with the corresponding parameters from $P_c = [p_0, p_1, p_2, \dots, p_{L-1}]$. Therefore, the designed color curve rendering function $\psi_c(\cdot)$ can be formulated as:

$$\psi_c(I_{fore}^c, P_c) = \frac{1}{\sum_{j=0}^{L-1} p_j} \sum_{i=0}^{L-1} p_i \xi \left(x - \frac{i}{L} \right), \quad x \in I_{fore}^c,$$

$$\text{where } \xi(y) = \begin{cases} 0, & y < 0 \\ y, & 0 \leq y < 1 \\ 1, & y > 1 \end{cases} \quad (1)$$

Hence, the final image can be represented as: $I_{final} = \Psi(I_{fore}, P) + I_{back}$, where $\Psi(I_{fore}, P) = \{\psi_r(I_{fore}^r, P_r), \psi_g(I_{fore}^g, P_g), \psi_b(I_{fore}^b, P_b)\}$.

Semantic CRM Previous methods (Cong et al. 2020; Cun and Pun 2020a) intend to obtain a unified harmonization model for any foreground images without any specific semantic knowledge. However, the semantic information is also important for the image harmonization (Tsai et al. 2017; Sofiiuk, Popenova, and Konushin 2021) and it does not make sense if we apply the same style to harmonize different categories (e.g. *Car* and *Person*). Since we have supposed that the linear layers in the color rendering module contain the

domain knowledge of the foreground, we make a further step of CRM via the curve rendering with extra semantic label of the foreground object.

As shown in Figure 2, given the semantic label d of the foreground region, we first embed the labels using a two-layer Multilayer Perceptron (MLP), obtaining the domain-specific label representations D . Then, we concatenate the style representations extracted by the network Φ and the label representations D in the semantic-aware CRM.

In practice, we analyze the categories of the foreground regions in iHarmony4 and divide it into 5 classes as guidance, including *Person*, *Vehicle*, *Animal*, *Food* and others. More details can be found in the supplementary materials.

Cascaded CRM/SCRM It is natural for the image editing tools to adjust the images with multiple steps for better visual quality. Inspired by this phenomenon, we extend our CRM (or SCRM) via the cascaded refinements. To reduce the inference time and learn a compact model, we keep the global features from the backbone unchanged and generate multi-stage heads and give the supervisions of each stage.

As shown in Figure 2, given the global foreground features F_f and background features F_b from the backbone, we firstly generate P_0 via a CRM and get its rendered image I_0 using $\Psi_c(I_{fore}^c, P_0)$. Then, we use another set of linear layers to predict the parameters P_n from the same global features (F_f, F_b) and rendering the curve using the previous prediction I_{n-1} via $\Psi_c(I_{n-1}, P_n)$. We set n equals to 2 to ensure the fast inference as efficiency as well as the high harmonization quality.

Discussion The proposed curve rendering modules make a new direction of the image harmonization that models could be also flexible and extendable. Besides, benefit from the proposed CRMs, all our methods are highly efficient and are able to handle the image harmonization in any resolutions without degrading the harmonization performance or speed.

Loss Function

We consider image harmonization as a supervised problem. Specifically, we measure the difference between the target and the corresponding rendered images (for each stage) in the composited region. Thus, we use relative L_1 loss between the predicted foreground and the target via the foreground mask M . Besides, for better visual quality, we also leverage the adversarial loss (Goodfellow et al. 2014) to our framework. We give the details of each part as follows.

Relative L_1 Loss \mathcal{L}_{pixel} Our method only need to measure the difference between the foreground of the predicted image and the target. Thus, inspired by recent works in watermark removal (Hertz et al. 2019; Cun and Pun 2020b), we only perform the pixel-wise L_1 loss function in the foreground region M , which restricts the network to learn the color curve of the foreground. Specifically, giving the rendered images I_n in each stage, we calculate the relative L_1 loss over the masked region:

$$\mathcal{L}_{pixel} = \sum_{n=1}^N \frac{\|M \times I_n - M \times I_{gt}\|_1}{sum(M)} \quad (2)$$

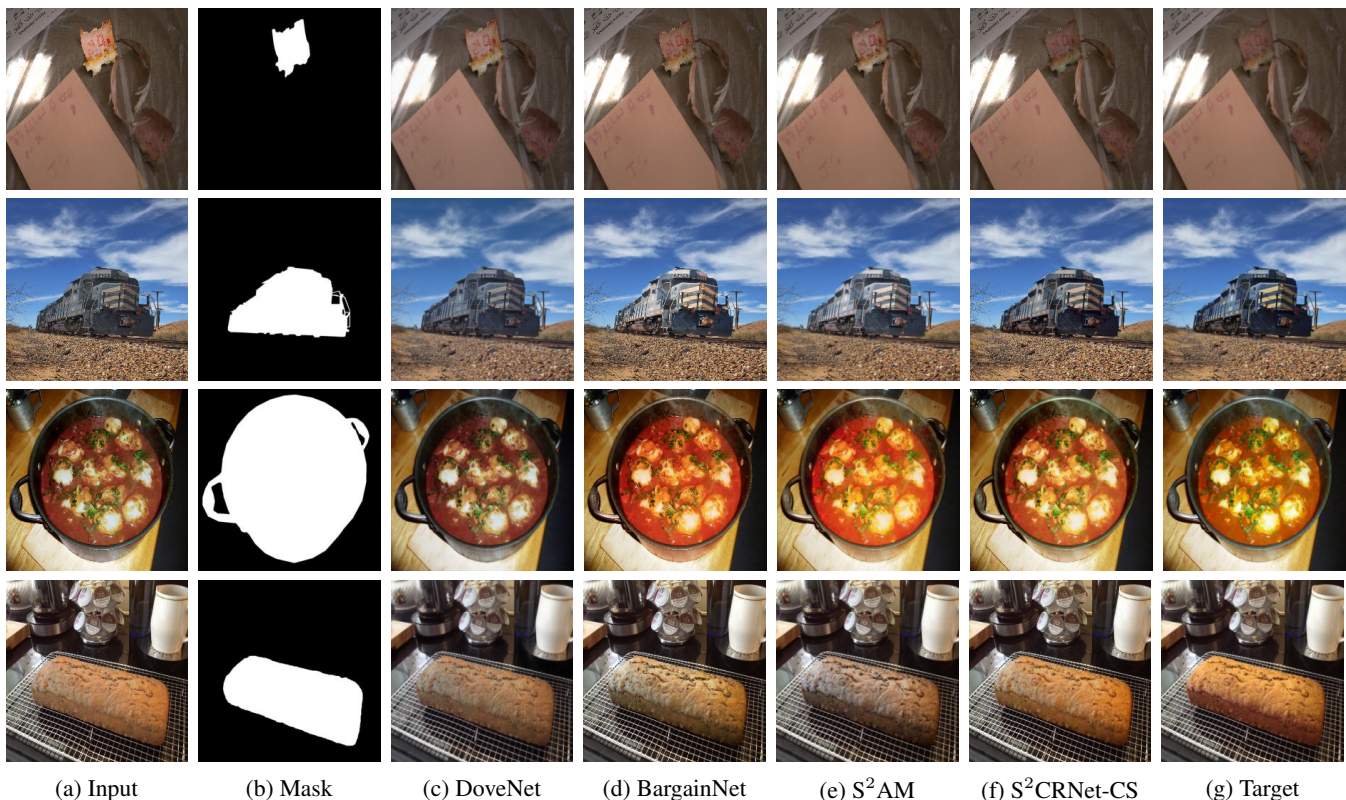


Figure 4: Comparisons with other methods on iHarmony4 Dataset.

Sub-dataset		HCOCO		HAdobe5k		HFlickr		Hday2night		All	
Evaluation metric	# Param.	MSE↓	PSNR↑	MSE↓	PSNR↑	MSE↓	PSNR↑	MSE↓	PSNR↑	MSE↓	PSNR↑
Input Composition	-	69.37	33.94	345.54	28.16	264.35	28.32	109.65	34.01	172.47	31.63
(Lalonde and Efros 2007)	-	110.10	31.14	158.90	29.66	329.87	26.43	199.93	29.80	150.53	30.16
(Xue et al. 2012)	-	77.04	33.32	274.15	28.79	249.54	28.32	190.51	31.24	155.87	31.40
(Zhu et al. 2015)	-	79.82	33.04	414.31	27.26	315.42	27.52	136.71	32.32	204.77	30.72
DIH(Tsai et al. 2017)	41.76M	51.85	34.69	92.65	32.28	163.38	29.55	82.34	34.62	76.77	33.41
DoveNet(Cong et al. 2020)	54.76M	36.72	35.83	52.32	34.34	133.14	30.21	54.05	35.18	52.36	34.75
S ² AM(Cun and Pun 2020a)	66.70M	33.07	36.09	48.22	35.34	124.53	31.00	48.78	35.60	48.00	35.29
BargainNet(Cong et al. 2021)	58.74M	24.84	37.03	39.94	35.34	97.32	31.34	50.98	35.67	37.82	35.88
IIH(Guo et al. 2021)	40.86M	<u>24.92</u>	37.16	43.02	35.20	<u>105.13</u>	31.34	55.53	35.96	<u>38.71</u>	35.90
RainNet(Ling et al. 2021)	54.75M	31.12	36.59	<u>42.84</u>	36.20	117.59	31.33	47.24	36.12	44.50	35.87
S ² CRNet	0.72M	29.28	37.51	46.70	35.67	122.16	31.37	52.79	36.82	45.17	36.27
S ² CRNet-C	<u>0.92M</u>	28.74	<u>37.55</u>	46.90	35.69	115.68	<u>31.49</u>	46.51	35.99	44.08	<u>36.41</u>
S ² CRNet-CS	0.95M	28.25	37.65	44.52	<u>35.93</u>	115.46	31.63	53.33	<u>36.28</u>	43.20	36.45

Table 1: Comparisons on iHarmony4. The best and the second best are marked as boldface and underline respectively.

where $N = 2$ is the total iteration in the *Cascaded-CRM* empirically.

Adversarial Loss \mathcal{L}_{adv} By considering the proposed S²CRNet as the generator G , we also utilize an additional discriminator D to identify the naturalness of the color. In detail, we use a standard 5 layers CONV-BN-RELU discriminator (Zhu et al. 2017) and leverage a least squares GAN (Mao et al. 2017) as criteria. Then, the generator is learnt to fool the discriminator and the discriminator is trained to identify the real or fake feed images iteratively.

Overall, our algorithm can be trained in an end-to-end

function via the combination of the losses above:

$$\mathcal{L}_{all} = \lambda_{pixel}\mathcal{L}_{pixel} + \lambda_{adv}\mathcal{L}_{adv} \quad (3)$$

where all the hyper-parameters (λ_{pixel} and λ_{adv}) are empirically set to 1 for all our experiments.

Experiments

Implementation Details

We implement our method in Pytorch (Paszke et al. 2017) and train on a single NVIDIA TITAN V GPU with 12GB memory. Our model is trained on 20 epochs with the batch

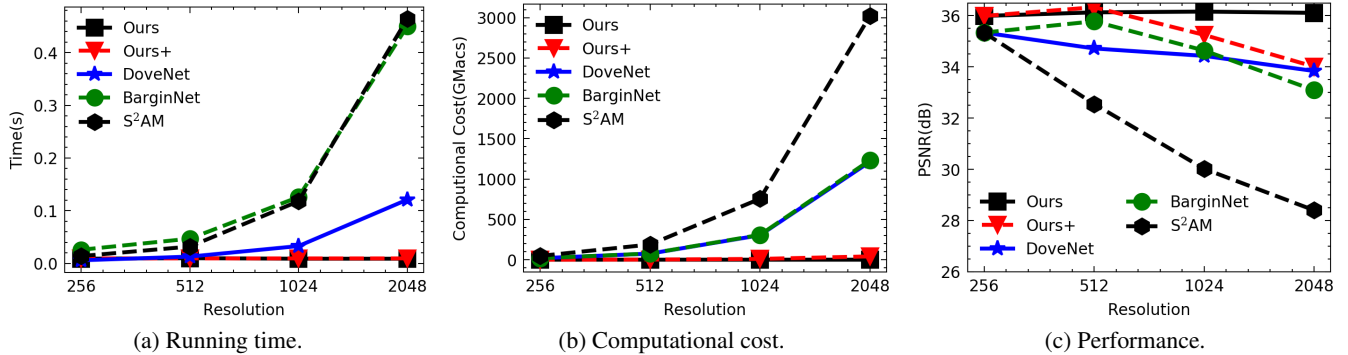


Figure 5: The influence of the image resolution from different aspects.

size of 8. All the images are resized to 256×256 and random cropped and flipped for fair training and evaluation as previous methods (Cong et al. 2020; Cun and Pun 2020a). We leverage the AdamW optimizer (Loshchilov and Hutter 2018) with the learning rate of 2×10^{-4} , the weight decay value of 10^{-2} and momentum of 0.9.

Following previous works (Cun and Pun 2020a; Tsai et al. 2017; Cong et al. 2020), we train our model on the benchmark dataset iHarmony4 (Cong et al. 2020) and test on the test set of iHarmony4 and the real-world test set in DIH (Tsai et al. 2017) (DIH99). The iHarmony4 consists of 4 sub-datasets (HCOCO, HAdobe5k, HFlickr, Hday2night) and includes 73146 image pairs for image harmonization including the synthesized images, the corresponding foreground masks and the target images. DIH99 only contains 99 real copy-paste samples with its foreground mask. As for evaluation, we validate our approaches on the iHarmony4 using Mean-Square-Errors (MSE) and Peak Signal-to-Noise Ratio (PSNR) as criteria metrics. Since DIH99 does not contain the target images, we conduct the subjective experiments.

Comparison with Existing Methods

Performance Comparison on iHarmony4. We compare the three variants of the proposed methods with different CRM, including S²CRNet (CRM), S²CRNet-C (Cascaded CRM) and S²CRNet-CS (Cascaded SCRNet, where the semantic labels are generated by a pre-trained segmentation model (Zhou et al. 2018)), with other state-of-the-art image harmonization algorithms, including DoveNet, S²AM, BargainNet, IIH (Guo et al. 2021), RainNet (Ling et al. 2021), *etc.*. All previous methods are tested using their official implementations and pre-trained models for fair comparison. As shown in Table 1, while training and testing on 256×256 limits the high-resolution performance, our S²CRNet still outperforms other methods in PSNR metric, which demonstrates the effectiveness of the global rendering curves. Also, the harmonization performance are gradually and significantly improved by each variant of the proposed CRMs. Compared with other encoder-decoder networks, the proposed method achieves state-of-the-art performance using only 2% parameters and runs faster than other methods even on high-resolution images, which will be discussed later.

Besides the numeric comparison, our proposed method

also obtains better visual quality than others. Qualitative examples in Figure 4 also show that the proposed method can generate harmonized results that are more realistic than other methods, which further indicates the benefits of the proposed CRM modules. More visual comparisons are presented in the supplementary materials.

High-Resolution Image Harmonization. We conduct extra experiments on the HAdobe5k sub-dataset in iHarmony4 for higher-resolution image harmonization. For comparison, we resize the source images with the square resolution of 256, 512, 1024 and 2048, and test the average processing time, computational cost and PSNR scores on the same hardware platform.

Since other state-of-the-art methods (DoveNet, BargainNet, S²AM) employ the fully convolutional encoder-decoder structure, they can be tested directly in higher resolution. As for our method, we make two choices of the proposed S²CRNet-CS. As shown in Table 5, in "Ours", we compute the curve on thumbnail inputs and render the full resolution images as Figure 2. Whereas in "Ours+", we directly use the high-resolution images as inputs to generate global curve parameters.

As shown in Figure 5a and Figure 5b, the speed and the computational cost of other methods grow rapidly as the image resolutions increase. However, both Ours and Ours+ require negligible additional resources to the original network and achieve up to $12 \times$ speedup compared to BargainNet and S²AM. In terms of the harmonization quality, there are also some interesting phenomena. As shown in Figure 5c, most of other methods confront a significant performance decline with the resolution increasing, especially S²AM. It might be because the encoder-decoder based structure will produce different reception fields of original images and then downgrade its performance. Differently, the global curve is resolution-free. "Ours" keeps the performance unchanged and "Ours+" only shows the minimal performance decrease.

Method	Input	DIH	DoveNet	BargainNet	Ours
Total votes	224	385	403	328	442
Preference	12.57%	21.60%	22.62%	18.41%	27.80%

Table 2: User study on DIH99 test set.

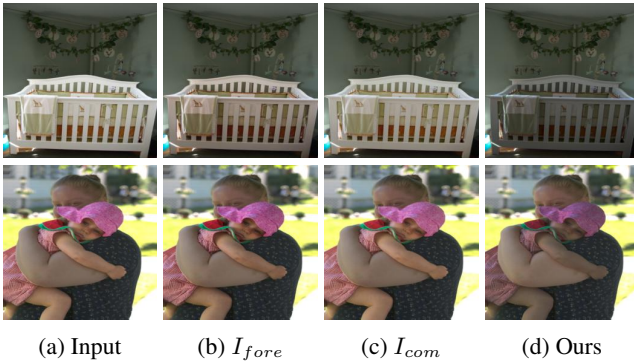


Figure 6: The influence of different encoder designs.

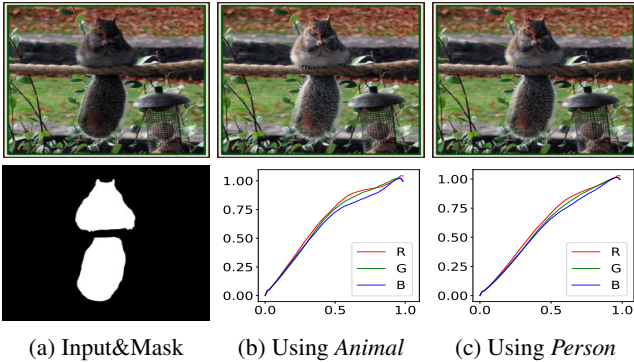


Figure 7: Results and rendering curves of SCRMs using different foreground semantic labels (*Person*, *Animal*).

User Study on DIH99. Since the real-wold image composition is still different from the synthesized dataset, we evaluate the proposed method and existing methods (DIH, DoveNet, BarginNet) by subjective experiments on DIH99. In detail, we randomly shuffle the displaying order of all the images and invite 18 users to select the most realistic results. As shown in Table 2, the proposed method gets the most votes with faster inference time and fewer model parameters as discussed previously. For visual comparison, we show the evaluation examples in the supplementary materials.

Ablation Studies

We conduct the ablation experiments to demonstrate the effectiveness of each component in the proposed S²CRNet, including the loss function, the effect of spatial-separated encoder and the CRMs. All the experiments are performed on both HCOCO and iHarmony4 with same configurations.

Loss Function. As shown in Table 3 Model *A* to *C*, we compare the performance on different loss functions. Since background and foreground domains are different, restricting the loss function on the masked region only using relative L_1 (rL_1) rather than L_1 loss helps a lot. Besides, L_{adv} are used to improve the realism of the predicted result.

Encoder Design *E*. Extracting and learning the global foreground and background features individually and foreground background feature concatenation (Ours in Model

#	Loss		Network		HCOCO		iHarmony	
	\mathcal{L}_{pixel}	\mathcal{L}_{adv}	<i>E</i>	CRM	MSE ↓	PSNR ↑	MSE ↓	PSNR ↑
-	Original Input				69.37	33.94	172.47	31.63
<i>A</i>	L_1		Ours	✓	67.64	34.08	114.65	32.11
<i>B</i>	rL_1		Ours	✓	28.43	37.59	46.79	36.20
<i>C</i>	rL_1	✓	Ours	✓	29.45	37.51	45.17	36.27
<i>D</i>	rL_1	✓	I_{fore}	✓	34.62	36.98	79.73	34.57
<i>E</i>	rL_1	✓	I_{com}	✓	58.53	34.69	88.61	33.88
<i>F</i>	rL_1	✓	Ours	<i>C</i>	28.47	37.60	44.08	36.41
<i>G</i>	rL_1	✓	Ours	<i>CS</i>	27.40	37.72	43.20	36.45

Table 3: Ablation studies.

C) are also the keys to facilitate the performance of the whole framework. As shown in Table 3 and Figure 6, compared with other alternatives that extract the global features using the foreground pixel only (I_{fore} in Model *D*) and the full image (I_{com} in Model *E*), spatial-separated encoder shows a much better performance.

CRMs. The numerical metrics of different CRMs have been listed in Table 1 and Table 3, both *Cascaded*-CRM (Model *F*) and *Cascaded*-SCRMs (Model *G*) hugely improve the base model (Model *E*). To further explore the influence of each variants, firstly, we show the importance of semantic labels. As shown in Figure 7, different semantic labels will produce different style curves under the same input. Then, for cascaded refinement, in Figure 8, cascaded refinement will produce different curves and give better performance. Finally, the global color curves also enable the proposed method to harmonize with domain-aware features from novel images. In Figure 8, a novel background can also guide the foreground regions harmonization.

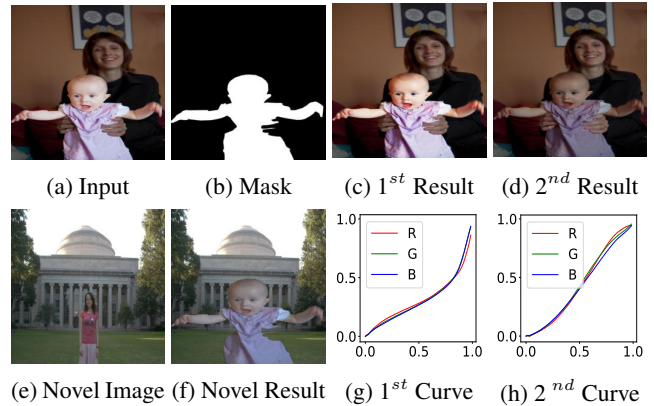


Figure 8: Given a composite image (a) and its mask (b), Cascaded-CRM learns to generate different harmonization results (c, d) via curves (g, h). Also, our method can harmonize the current foreground via novel backgrounds (e, f).

Conclusion

In this paper, instead of the pixel-wise image harmonization, we consider it as a global curve learning problem for the first time. To this end, we present Spatial-separated Curve Rendering Network (S²CRNet) for efficient and high-resolution image harmonization. In detail, the proposed method extract the global spatial-separated features for the foreground

and background using an efficient backbone. After that, the region-aware features are learnt individually and are combined to generate the parameters of curve function. Finally, we render the original foreground using these parameters. Besides, we extend this method to cascaded refinement and semantic-aware prediction. Experiments show the superior of the proposed methods especially on the model efficiency and high-resolution inputs.

References

- Bychkovsky, V.; Paris, S.; Chan, E.; and Durand, F. 2011. Learning photographic global tonal adjustment with a database of input/output image pairs. In *CVPR*, 97–104. IEEE.
- Cohen-Or, D.; Sorkine, O.; Gal, R.; Leyvand, T.; and Xu, Y.-Q. 2006. Color harmonization. In *SIGGRAPH*, 624–630.
- Cong, W.; Niu, L.; Zhang, J.; Liang, J.; and Zhang, L. 2021. BargainNet: Background-Guided Domain Translation for Image Harmonization. In *ICME*.
- Cong, W.; Zhang, J.; Niu, L.; Liu, L.; Ling, Z.; Li, W.; and Zhang, L. 2020. Dovenet: Deep image harmonization via domain verification. In *CVPR*, 8394–8403.
- Cun, X.; and Pun, C.-M. 2020a. Improving the harmony of the composite image by spatial-separated attention module. *TIP*, 29: 4759–4771.
- Cun, X.; and Pun, C.-M. 2020b. Split then Refine: Stacked Attention-guided ResUNets for Blind Single Image Visible Watermark Removal. *AAAI*.
- Deng, J.; Dong, W.; Socher, R.; Li, L.-J.; Li, K.; and Fei-Fei, L. 2009. Imagenet: A large-scale hierarchical image database. In *CVPR*, 248–255. Ieee.
- Gharbi, M.; Chen, J.; Barron, J. T.; Hasinoff, S. W.; and Durand, F. 2017. Deep bilateral learning for real-time image enhancement. *TOG*, 36(4): 1–12.
- Goodfellow, I. J.; Pouget-Abadie, J.; Mirza, M.; Xu, B.; Warde-Farley, D.; Ozair, S.; Courville, A.; and Bengio, Y. 2014. Generative adversarial networks. *arXiv preprint arXiv:1406.2661*.
- Guo, Z.; Zheng, H.; Jiang, Y.; Gu, Z.; and Zheng, B. 2021. Intrinsic Image Harmonization. In *CVPR*, 16367–16376.
- Hao, G.; Iizuka, S.; and Fukui, K. 2020. Image Harmonization with Attention-based Deep Feature Modulation. In *BMVC*.
- Hertz, A.; Fogel, S.; Hanocka, R.; Giryas, R.; and Cohen-Or, D. 2019. Blind visual motif removal from a single image. In *CVPR*, 6858–6867.
- Howard, A. G.; Zhu, M.; Chen, B.; Kalenichenko, D.; Wang, W.; Weyand, T.; Andreetto, M.; and Adam, H. 2017. Mobilenets: Efficient convolutional neural networks for mobile vision applications. *arXiv preprint arXiv:1704.04861*.
- Hu, Y.; He, H.; Xu, C.; Wang, B.; and Lin, S. 2018. Exposure: A white-box photo post-processing framework. *TOG*, 37(2): 1–17.
- Hu, Y.; Wang, B.; and Lin, S. 2017. FC4: Fully Convolutional Color Constancy with Confidence-weighted Pooling. In *CVPR*, 4085–4094.
- Iandola, F. N.; Han, S.; Moskewicz, M. W.; Ashraf, K.; Dally, W. J.; and Keutzer, K. 2016. SqueezeNet: AlexNet-level accuracy with 50x fewer parameters and; 0.5 MB model size. *arXiv preprint arXiv:1602.07360*.
- Isola, P.; Zhu, J. Y.; Zhou, T.; and Efros, A. A. 2017. Image-to-image translation with conditional adversarial networks. In *CVPR*, volume 2017-Janua, 5967–5976. ISBN 9781538604571.
- Jia, J.; Sun, J.; Tang, C.-K.; and Shum, H.-Y. 2006. Drag-and-drop pasting. *TOG*, 25(3): 631–637.
- Lalonde, J.-F.; and Efros, A. A. 2007. Using color compatibility for assessing image realism. In *ICCV*, 1–8. IEEE.
- Lee, D.; Pfister, T.; and Yang, M.-H. 2019. Inserting videos into videos. In *CVPR*, 10061–10070.
- Lin, T.-Y.; Maire, M.; Belongie, S.; Hays, J.; Perona, P.; Ramanan, D.; Dollár, P.; and Zitnick, C. L. 2014. Microsoft coco: Common objects in context. In *ECCV*, 740–755.
- Ling, J.; Xue, H.; Song, L.; Xie, R.; and Gu, X. 2021. Region-Aware Adaptive Instance Normalization for Image Harmonization. In *CVPR*, 9361–9370.
- Loshchilov, I.; and Hutter, F. 2018. Fixing weight decay regularization in adam.
- Mao, X.; Li, Q.; Xie, H.; Lau, R. Y.; Wang, Z.; and Paul Smolley, S. 2017. Least squares generative adversarial networks. In *ICCV*, 2794–2802.
- Paszke, A.; Gross, S.; Chintala, S.; Chanan, G.; Yang, E.; DeVito, Z.; Lin, Z.; Desmaison, A.; Antiga, L.; and Lerer, A. 2017. Automatic differentiation in pytorch.
- Pérez, P.; Gangnet, M.; and Blake, A. 2003. Poisson image editing. In *SIGGRAPH*, 313–318.
- Reinhard, E.; Adhikhmin, M.; Gooch, B.; and Shirley, P. 2001. Color transfer between images. *CG&A*, 21(5): 34–41.
- Ronneberger, O.; Fischer, P.; and Brox, T. 2015. U-net: Convolutional networks for biomedical image segmentation. In *MICCAI*, 234–241. Springer.
- Sofiiuk, K.; Popenova, P.; and Konushin, A. 2021. Foreground-aware Semantic Representations for Image Harmonization. In *WACV*, 1620–1629.
- Sunkavalli, K.; Johnson, M. K.; Matusik, W.; and Pfister, H. 2010. Multi-scale image harmonization. *TOG*, 29(4): 1–10.
- Tsai, Y.-H.; Shen, X.; Lin, Z.; Sunkavalli, K.; Lu, X.; and Yang, M.-H. 2017. Deep image harmonization. In *CVPR*.
- Xue, S.; Agarwala, A.; Dorsey, J.; and Rushmeier, H. 2012. Understanding and improving the realism of image composites. *TOG*, 31(4): 1–10.
- Yu, H.; Chen, K.; Wang, K.; Qian, Y.; Zhang, Z.; and Jia, K. 2020. Cascading Convolutional Color Constancy. In *AAAI*.
- Zeng, H.; Cai, J.; Li, L.; Cao, Z.; and Zhang, L. 2020. Learning image-adaptive 3D lookup tables for high performance photo enhancement in real-time. *TPAMI*.
- Zhou, B.; Zhao, H.; Puig, X.; Xiao, T.; Fidler, S.; Barriuso, A.; and Torralba, A. 2018. Semantic understanding of scenes through the ade20k dataset. *IJCV*.

Zhou, H.; Hadap, S.; Sunkavalli, K.; and Jacobs, D. W. 2019. Deep Single Portrait Image Relighting. In *ICCV*.

Zhu, J.-Y.; Krahenbuhl, P.; Shechtman, E.; and Efros, A. A. 2015. Learning a discriminative model for the perception of realism in composite images. In *ICCV*, 3943–3951.

Zhu, J.-Y.; Park, T.; Isola, P.; and Efros, A. A. 2017. Unpaired Image-to-Image Translation using Cycle-Consistent Adversarial Networks. *ICCV*.

Supplementary Material

The Details of Semantic Labels Extraction.

In the proposed semantic curve rendering module (SCRM), correct foreground semantic label benefits the performance of image harmonization. However, iHarmony4 (Cong et al. 2020) do not contain the ground truth labels of the foreground. To obtain the semantic labels, firstly, we get the categories in HCOCO sub-dataset via COCO API (Lin et al. 2014). For the rest sub-datasets, we leverage a semantic segmentation model in (Zhou et al. 2018) to segment the composite images. Then, we choose the segmented region which has maximal intersection with the foreground mask, and consider it as the category label. Finally, we get the distributions of the foreground labels as summarized in Table 4. Thus, we roughly divide the foreground regions into 5 categories, including *Person*, *Vehicle*, *Animal*, *Food* and others. We argue that this setting is also suitable for the daily usages.

Classes	HCOCO	HAdobe5k	HFlickr	Hday2night	iHarmony4
Person	13416	7274	1629	0	22319
Vehicle	4434	1338	808	10	6590
Animal	7274	747	675	0	8696
Food	6752	280	721	0	7753
Others	10952	11958	4444	434	27788
Total	42828	21597	8277	444	73146

Table 4: Predicted foreground distributions in iHarmony4.

Influence of Different Foreground Ratios.

We show the quantitative results on iHarmony4 in different foreground ratio ranges. Following previous methods (Cong et al. 2020), we employ mean square error (MSE) and foreground mean square error (fMSE) as evaluation metrics, where fMSE measures the MSE scores of the harmonized foreground regions. The performance is reported in four different foreground ranges, including 0% to 5%, 5% to 15%, 15% to 100% and overall results. As shown in Table 5, the performance of all the models will be downgraded as the foreground ratios increase. Nevertheless, our S²CRNet achieve the best performance in most of the foreground ratio intervals. Especially, our model performs much better than state-of-art models on small foreground regions (0%-5%), outperforming around 150 in fMSE metric.

Visual Comparison on High-Resolution Images.

We visualize an example to show the influence of the input resolution. Similar to the high-resolution image harmonization experiments in the primary paper, we compare our

method with other related tasks in harmonizing images at different resolutions of the square of 256, 512, 1024 and 2048. Since our method will resize the input resolution to 256 and show the same results, here, we use the “Ours+” settings, which means we do not down-sampling the input and extract the global feature on the same resolution as others. As shown in Figure 9, the proposed method get more stable results, while others show different harmonized qualities as the resolutions change.

More Rendering Curves Visualization.

We present more visual results to visualize the preliminary rendering curves and the curves of cascaded refinements. As shown in Figure 10, the curves generated by the CRM are different according to various input samples, which demonstrates that the S²CRNet can produce the meaningful curve parameters for each images via the deep features. Also, for cascaded refinement, the curves in each stage are also different and these stage-aware curves contribute to the improvement of the harmonization performance according to the visualized results of different stages in Figure 10.

Visual Results on DIH99 Dataset.

As we have presented the user study in the main paper, here, we show the visual results on harmonizing real-world composite images on DIH99. We compare the harmonized results that generated from previous methods including DIH, DoveNet and BargainNet. As shown in Figure 11, our S²CRNet-CS can also achieve reliable results in the real dataset.

More Visual Results on iHarmony4 Dataset.

Given some composite images and their foreground masks, we present more harmonized results on iHarmony4 dataset by methods including S²AM (Cun and Pun 2020a), DoveNet (Cong et al. 2020), BargainNet (Cong et al. 2021) and our S²CRNet-CS in Figure 12. Compared with the other baselines, the S²CRNet-CS can generate more harmonious results that also maintain visual similarities with the target natural images.

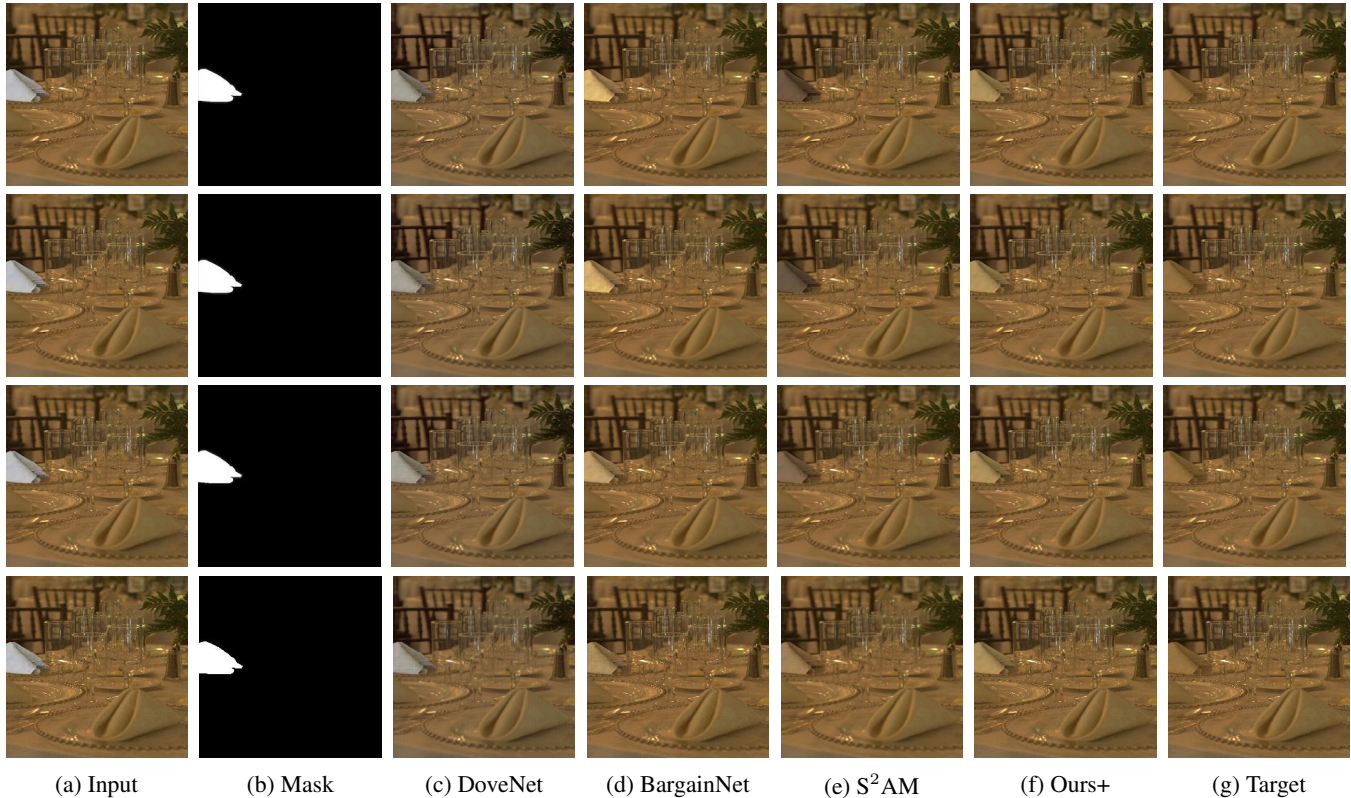


Figure 9: Qualitative comparisons with existing methods in harmonizing images at different resolutions. Here, we resize the all the images to the same resolutions for presentation. The original input images are 256×256 , 512×512 , 1024×1024 , 2048×2048 from the bottom up successively.

Foreground Ratios	0%-5%		5%-15%		15%-100%		0%-100%	
Evaluation metric	MSE ↓	fMSE ↓	MSE ↓	fMSE ↓	MSE ↓	fMSE ↓	MSE ↓	fMSE ↓
Input composition	28.51	1208.86	119.19	1323.23	577.58	1887.05	172.47	1387.30
(Lalonde and Efros 2007)	41.52	1481.59	120.62	1309.79	444.65	1467.98	150.53	1433.21
(Xue et al. 2012)	31.24	1325.96	132.12	1459.28	479.53	1555.69	155.87	1411.40
(Zhu et al. 2015)	33.30	1297.65	145.14	1577.70	682.69	2251.76	204.77	1580.17
DIH(Tsai et al. 2017)	18.92	799.17	64.23	725.86	228.86	768.89	76.77	773.18
DoveNet(Cong et al. 2020)	14.03	591.88	44.90	504.42	152.07	505.82	52.36	549.96
S ² AM(Cun and Pun 2020a)	13.51	509.41	41.79	454.21	137.12	449.81	48.00	481.79
BargainNet(Cong et al. 2021)	10.55	450.33	32.13	359.49	109.23	353.84	37.82	405.23
RainNet(Ling et al. 2021)	11.66	550.38	32.05	378.69	117.41	389.81	40.29	469.61
S ² CRNet-CS	8.42	301.97	29.74	336.24	126.56	405.13	43.21	336.99

Table 5: Foreground Harmonization Comparisons on iHarmony4. The fMSE measures the mean square error scores of the harmonized foreground regions. The best results are marked as bold.

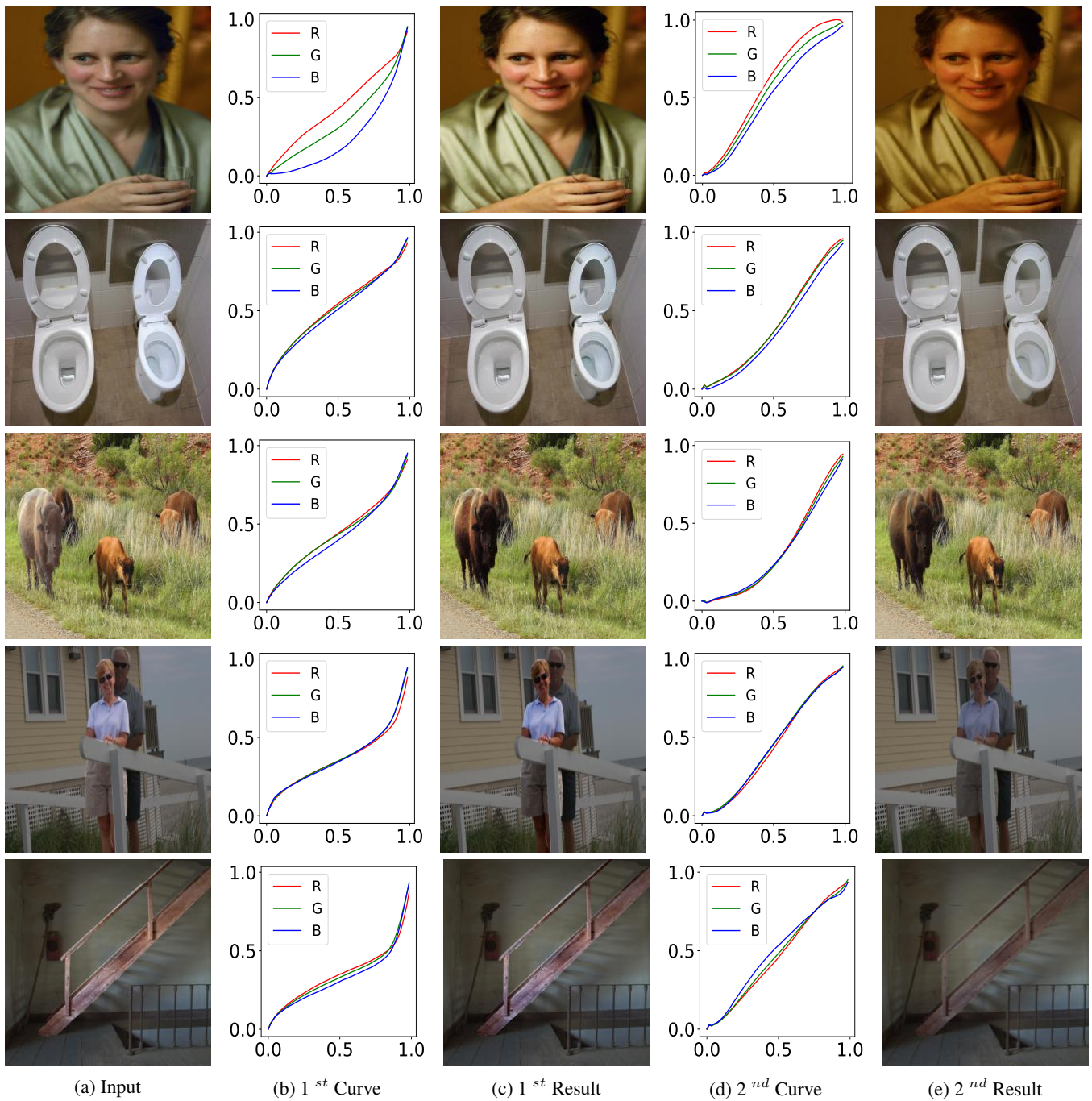
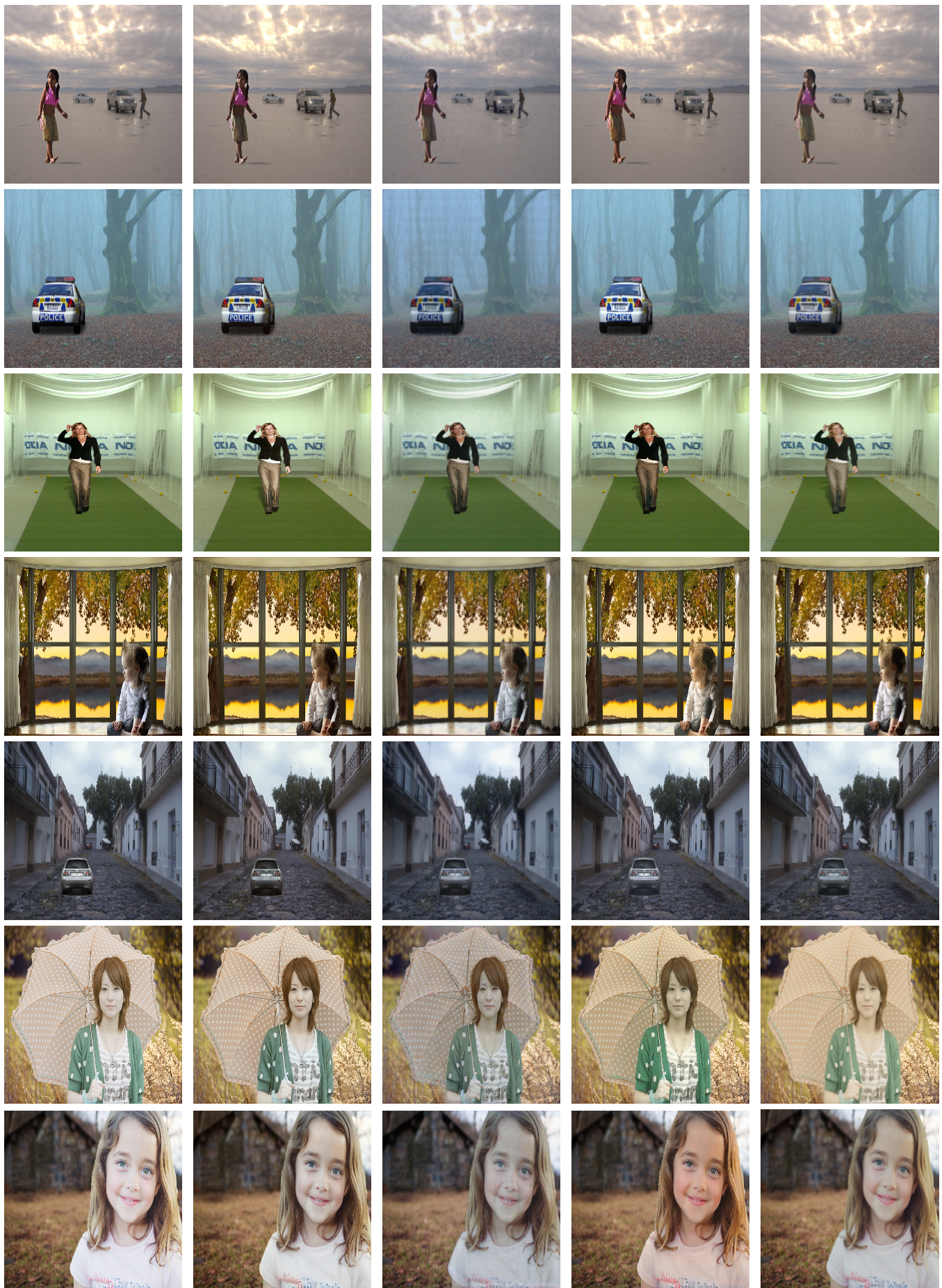


Figure 10: More visualized results of the cascaded rendering curves generated by S^2 CRNet.



(a) Input

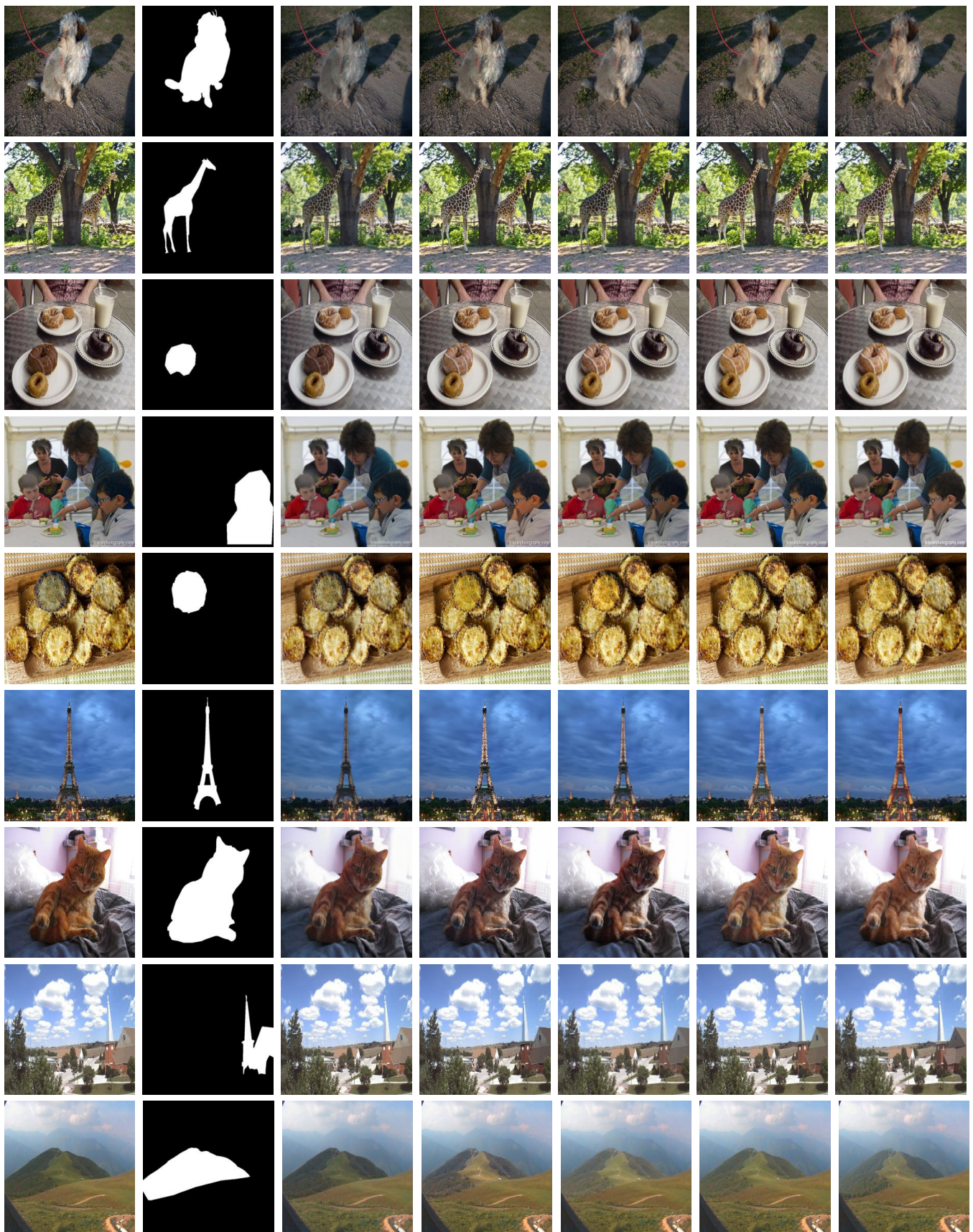
(b) DIH

(c) DoveNet

(d) BargainNet

(e) S²CRNet-CS

Figure 11: More comparisons between our method and other state-of-the-art methods over DIH99 dataset.



(a) Input

(b) Mask

(c) DoveNet

(d) BargainNet

(e) S²AM

(f) S²CRNet-CS

(g) Target

Figure 12: Comparison with other methods on iHarmony4 Dataset.